Proceedings of the Canadian Society for Mechanical Engineering International Congress
32nd Annual Conference of the Computational Fluid Dynamics Society of Canada
Canadian Society of Rheology Symposium
CSME/CFDSC/CSR 2025
May 25–28, 2025, Montréal, Québec, Canada

Evaluating Train-Induced Wind Power Potential in Vancouver's SkyTrain System: A Case Study at Burrard Station

Lisha Tan[1], Yunbo Nie[1], Mohammad Rahnama[1],

[1]Department of Energy Management, New York Institute of Technology, Vancouver, Canada

Jan.27th, 2025

***Abstract*—**This study explores the feasibility of harvesting train-induced airflows as a renewable energy source in Vancouver's SkyTrain metro stations, with Burrard Station serving as the primary test site. Field data were collected using high-precision anemometers to measure airflow patterns, and Fast Fourier Transform (FFT) analysis identified four airflow phases— pre-compression, piston effect, slipstream, and wake—with peak velocities up to 6 m/s. Dirichlet Process Mixture Models (DPMM) were employed to characterize wind speed distributions. A small Archimedes-type turbine was tested under controlled conditions, achieving a maximum output of 202.5 mW and motor efficiencies ranging from 20.3% to 59.0%. Economic feasibility analyses, performed via RETScreen, revealed capacity factors of 25.01% for the Burrard–to–King George route and 10.84% for the Burrard–to–Waterfront route, but also highlighted extended payback periods (50–133 years) and negative internal rates of return (-5.7% to -12.1%). Nevertheless, the system demonstrated a 93% reduction in carbon emissions, aligning with Vancouver's climate objectives. This work underscores the potential environmental benefits of train-induced wind energy in urban transit infrastructure, while calling attention to the need for improved turbine designs, cost-reduction strategies, and supportive policy frameworks.

***Keywords-component*—Train-induced wind energy; renewable energy; SkyTrain; RETScreen**

I. Introduction

As urban populations grow, the demand for sustainable public transportation intensifies. Metro systems, while energy-intensive, generate unique aerodynamic conditions through train movements, offering untapped potential for renewable energy generation. The "piston effect"—air displacement caused by trains in confined tunnels—creates high-velocity airflow that can drive small-scale wind turbines. Early work by Cross [1] underscored how strategic tunnel design and ventilation can amplify these airflow patterns, indicating that suitably scaled turbines may convert train-induced wind into electrical power.

This work was funded by New York Institute of Technology.

Multiple investigations have examined various turbine configurations in subterranean or semi-enclosed railway environments. For instance, Utomo [2] installed a 0.5 m-diameter Savonius turbine along railway tracks and reported a maximum output of 6.4 W at an average wind velocity of 5.7 m/s—demonstrating that intermittent, train-generated airflow can yield continuous energy capture if properly sited. Bethi [3] refined Savonius turbine geometries within Singapore's Mass Rapid Transit tunnels by optimizing blade curvature and overlap ratios, achieving higher aerodynamic efficiency despite limited cross-sectional space. Beyond conventional rotor-based designs, Zheng [4] introduced a hybrid turbine–vibrating system within 5–6 m diameter tunnel segments in Chengdu's subway. At wind speeds of around 7 m/s, this system simultaneously drove a small wind turbine and piezoelectric elements, producing 59.31 mW—sufficient for low-energy devices like LED indicators and sensors.

Collectively, these studies indicate that train-induced airflow can be harnessed for power generation, but reported efficiencies vary widely based on turbine geometry, tunnel cross-section, and airflow velocity. Although several successful implementations have been documented in Asia and Europe, similar large-scale feasibility assessments are scarce in North American contexts.

Vancouver's commitment to climate action and its SkyTrain infrastructure, characterized by semi. enclosed tunnels and frequent train operations, presents a novel opportunity to investigate localized wind energy recovery. This study addresses critical gaps by (1) characterizing airflow patterns at Burrard Station using high-precision anemometry and Dirichlet Process Mixture Models (DPMM) (2) evaluating turbine designs compatible with SkyTrain's spatial constraints, and (3) assessing economic feasibility via RETScreen. By integrating field data, statistical modeling, and techno-economic analysis, this

work aims to establish a replicable framework for transforming transit infrastructure into renewable energy assets, contributing to global efforts in urban sustainability.

II. Methodology

A. Field Data Collection

Burrard Station was selected for in-depth analysis due to its unique multi-level layout and tunnel geometry, which generate complex wind patterns. To capture comprehensive wind data, measurements were taken from two distinct directions and multiple levels within the station. High-precision anemometers (BTMETER BT-866A Pro CFM) were mounted on tripods at different elevations—approximately one metre and two metres above the ground—to monitor airflow from both inbound(Burrard to Waterfront) and outbound directions(Burrard to King George) towards incoming trains. These instruments captured real-time wind speed, temperature, and humidity data during inbound and outbound stops.

Structural dimensions, including tunnel width, height, and curvature, were measured using a LEXIVON 2-in-1 digital laser tape to establish correlations with airflow patterns. Data collection was carried out at various times of the day to account for schedule variations, and each monitoring point was observed for at least 30 minutes to ensure data stability. Extended recordings were performed at key locations, and all data were transferred to a computer via USB for further analysis. The schematic diagram for the measurement protocol is illustrated in Fig. 1.

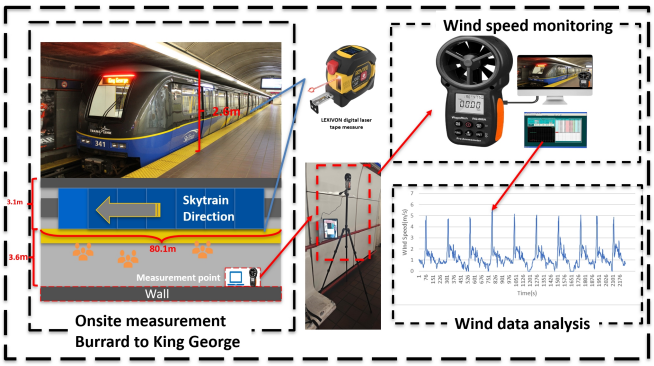

Figure. 1: Schematic Diagram for Field Data Collection

B. Wind Data Analysis

Feature Extraction

To characterize wind speed signals, we applied the Fast Fourier Transform (FFT) using Python libraries such as NumPy and SciPy 1.9.1. The FFT rapidly converts time-domain data to the frequency domain, revealing dominant periodic components in the airflow.

Statistical Modeling

The DPMM is used to derive the empirical probability density function (PDF) and the corresponding cumulative distribution function (CDF). This nonparametric technique dynamically determines the number of mixture components from the data, eliminating the need for a predefined model structure. By integrating the estimated PDFs, we obtain a data-driven CDF that represents the likelihood of a particular range of wind speeds within the station. For the simulated results, the team used the Kolmogorov-Smirnov test (K-S) to assess the accuracy of the model. This test compares the empirical wind speed distribution with the CDF derived from the model, quantifying any significant differences.

C. Evaluation of Wind Turbine Performance

Literature Reviews on Wind Turbine Performance

The research team evaluated vertical and horizontal-axis wind turbine designs based on cut-in speed, structural dimensions, and efficiency. This analysis provides a basis for identifying turbines suitable for integration into the station infrastructure, ensuring compatibility with operational requirements and passenger comfort.

Wind Turbine Power Coefficient Experiment

A small Archimedes-type wind turbine was chosen for further feasibility study due to its compact design and suitability for the turbulent airflow environment of the Burrard station. However, since its power profile was not readily available, the research team conducted an experiment to test its power curve.

An axial fan was used to generate controlled wind speeds ranging from 0 to 9.9 m/s. Wind speed at the turbine's disc area was measured using an anemometer, with recordings taken from 0 to 7.9 m/s. The turbine's electrical output was monitored using a multimeter connected in series with a fixed 100 Ω resistor. The electrical power P was calculated using:

$$P = I^2 R, \tag{1}$$

where I is the measured current and $R = 100\ \Omega$ is the known resistor.

The schematic diagram below steps are illustrated in Fig. 2. The key performance parameters of the fan literature review are also listed in Table I below.

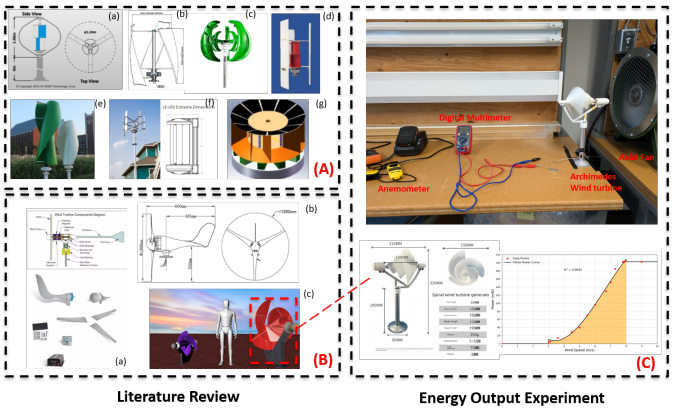

Figure. 2: Schematic Diagram of Literature Review and Energy Output Experiment Setup

TABLE. I Specifications of Wind Turbines

Model	Type	RatedPower(W)	Blade Dia./Height (m)	Cut-in Wind Speed (m/s)	MaxEfficiency (%)
DS-300 [5]	VAWT	300	1.24/1.06	3	15.1
ATO-X3-200 [6]	VAWT	200	0.55/0.75	2	32.0
ATO-X3-100 [7]	VAWT	100	0.55/0.75	2	22.9
XTL-R1-100W [8]	VAWT	100	0.9/0.6	2	22.7
HS-100 [9]	VAWT	100	0.55/0.8	1.5	21.5
FS-50 [10]	VAWT	50	0.4/0.9	1.3	17.0
RX-10V5 [11]	VAWT	10	0.328/0.3	2	16.6
LE-v50 Extreme [12]	VAWT	10	0.27/0.456	5	7.7
ATO-WT-S100 [13]	HAWT	100	1.2/–	2	14.4
AWM-750D-150W [15]	HAWT	125	0.75/–	3	26.7
Archimedes 10W [14]	HAWT	10	0.15/–	–	–
SHJ-50S [16]	HAWT	50	1.1/–	–	5.6

D. Energy Conversion and Feasibility Study

After constructing the CDFs from DPMM on the site wind data, hourly wind speeds (one for each operational hour of the SkyTrain, totaling 7,300 hours annually) are generated via an accept–reject sampling method [17]. Each sampled wind speed $v(t)$ then serves as the input for evaluating the available wind power, which is calculated as

$$P_{\text{wind}}(t) = \frac{1}{2}\,\rho\,A\,v(t)^3, \tag{2}$$

where $\rho = 1.225\ \text{kg/m}^3$ is the air density under standard conditions, and A is the rotor swept area, $0.018\ \text{m}^2$ per turbine in this case. To account for the actual electricity generation from the turbine, the power available in the wind $P_{\text{wind}}(t)$ is multiplied by a wind-speed-dependent power coefficient $C_p(v)$. Thus,

$$P_{\text{electric}}(t) = P_{\text{wind}}(t) \cdot C_p(v), \tag{3}$$

where $C_p(v)$ is defined through the experiment mentioned above.

To find the annual energy production, the electric power output is summed (or numerically integrated) over the entire 7,300-hour period:

$$E = \int_{t_1}^{t_2} P_{\text{electric}}(t)\,dt, \tag{4}$$

where t_1 and t_2 represent the start and end of the evaluation period, respectively.

Finally, once the total yearly energy E has been determined, the Capacity Factor (CF) is evaluated. The CF is the ratio of the annual energy production to the maximum possible energy if the turbine were operating at its rated power P_{rated} for every operational hour in the year (7,300 hours), expressed as a percentage:

$$\text{CF}\,(\%) = \frac{E}{P_{\text{rated}} \times 7300} \times 100. \tag{5}$$

After energy conversion, a preliminary feasibility study was conducted using RETScreen, incorporating local electricity pricing, installation costs, and potential maintenance expenses. Each selected turbine was assumed to have a rated capacity of 200 mW. A total of 500 turbines are envisioned to achieve an aggregate capacity of 1 kW, occupying approximately $8\ \text{m}^2$ without considering the interaction effects between turbines. Payback periods and greenhouse gas reductions were estimated based on projected capacity factors and Vancouver's electricity grid emissions intensity. Detailed RETScreen settings are provided in Table II.

TABLE. II RETScreen Climate and Financial Information.

Climate Information		Financial Information	
Parameter	**Value**	**Parameter**	**Value**
Latitude	49.3	Fuel Cost Escalation Rate	7%
Longitude	-123.1	Inflation Rate	2%
Climate Zone	4C - Mixed - Marine	Discount Rate	9%
Elevation (m)	3	Reinvestment Rate	9%
Heating Design Temperature (°C)	-0.5	Project Life (yr)	20
Cooling Design Temperature (°C)	24.3		
Earth Temperature Amplitude (°C)	17.8		

Pricing information was sourced from online procurement platforms, including Alibaba and other websites, and is listed in the Table III.

TABLE. III Cost Breakdown for Components.

Component	Cost (CAD)
PLA Material	8.97
Steel Pipe	0.13
Metal Plate	0.99
RV0.5 Wire	0.09
Brushless Motor	3.42
Rectifier	0.57
Manufacturing and Management	5.83
Total	**20.00**

III. Results

A. Station Geometry

The Table IV systematically documents the structural geometry of Burrard station, including cross-sectional dimensions of platforms in both directions and building parameters related to airflow. This illustrates the aerodynamic impact of station design on observed wind dynamics. This integration of methods for frequency domain analysis and geometric representation provides a powerful framework for assessing the interaction between transit operations and environmental fluid behavior.

TABLE. IV Station Dimensions for Burrard to Waterfront and Burrard to King George

Parameter	Burrard to Waterfront	Burrard to King George
Station Length (m)	79.7	80.1
Platform Height (m)	3.7	3.1
Platform Width (m)	3.7	3.6
Track Height (from platform up) (m)	3.0	2.6
Track Region Width (m)	3.0	3.1
Side Entrance Width (m)	5.0	5.0
Side Entrance Height (m)	2.3	2.3

B. Wind Speed Characterization

FFT results

To understand the periodicity of wind speed variations associated with different train dispatch frequencies, a FFT analysis was conducted on two specific routes: Burrard to Waterfront and Burrard to King George. The results of this analysis are shown in Fig. 3.

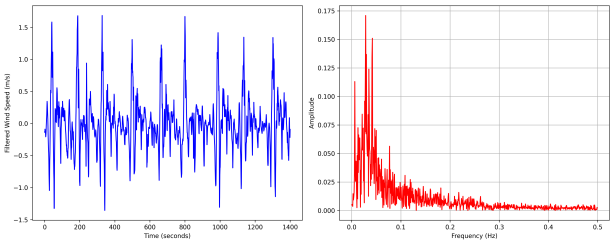

(a)Burrard to Waterfront

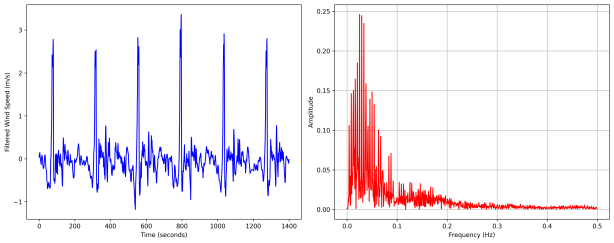

(b) Burrard to King George

Figure. 3: Comparison of FFT Analysis for Different Routes

Statistical Modeling Results

The statistical model results with curve fitting using DMPP are given in Table V and Fig. 4. These two functions are tested by K-S, and their P-values are greater than 0.05, which indicates their validity.

TABLE. V Statistically Derived Wind Speed Functions for Different Projects.

Direction	Statistically Wind Speed Function
Burrard to Waterfront	$f(x) \approx 0.432 \cdot e^{-0.5\frac{(x-1.180)^2}{0.101}} + 0.260 \cdot e^{-0.5\frac{(x-0.763)^2}{0.017}} + 0.001 \cdot e^{-0.5\frac{(x-1.134)^2}{0.319}} + 0.196 \cdot e^{-0.5\frac{(x-1.908)^2}{0.292}} + 0.001 \cdot e^{-0.5\frac{(x-1.135)^2}{0.318}} + 0.110 \cdot e^{-0.5\frac{(x-0.365)^2}{0.042}}$
Burrard to King George	$f(x) \approx 0.346 \cdot e^{-0.5\frac{(x-1.571)^2}{0.205}} + 0.045 \cdot e^{-0.5\frac{(x-4.390)^2}{0.393}} + 0.273 \cdot e^{-0.5\frac{(x-0.793)^2}{0.021}} + 0.035 \cdot e^{-0.5\frac{(x-2.044)^2}{0.477}} + 0.131 \cdot e^{-0.5\frac{(x-0.475)^2}{0.045}} + 0.171 \cdot e^{-0.5\frac{(x-1.193)^2}{0.065}}$

C. Archimedes-Type Turbine Power Profile

The power curve data through the experiment is given in Table VIand the equation for its coefficient c(v) through the polynomial regression method is found below:

$$c(v) = -1.844v^3 + 36.9v^2 - 187.4v + 290.4 \tag{6}$$

Subject to the following conditions:

$$c = 0.0, \quad \text{if } c < 0, \tag{7}$$

$$c = 100.0, \quad \text{if } c > 100. \tag{8}$$

The final value is:

$$c_{\text{final}} = \frac{c}{100.0} \tag{9}$$

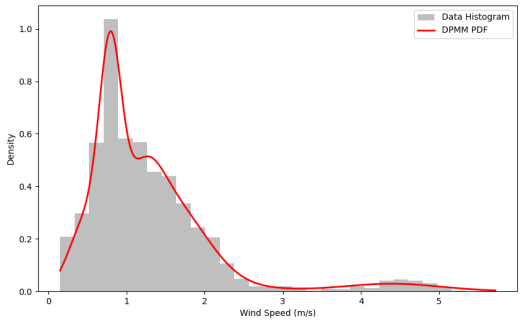

(a) Burrard to Waterfront

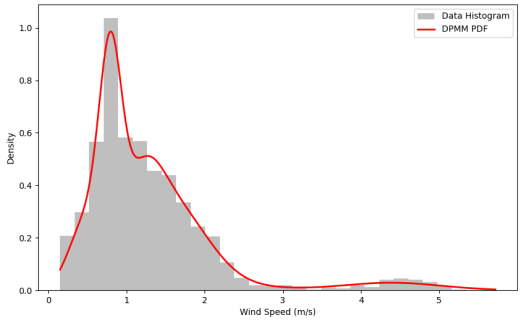

(b) Burrard to King George

Figure. 4: Two Curve-Fitting Results from Different Routes

TABLE. VI Power Output of Archimedes-type Wind Turbine at Various Wind Speeds.

Fan Speed (m/s)	Disc Area Speed (m/s)	Current (mA)	Power (mW)
0.0	0.0	0.0	0.0
4.1	3.1	7.0	4.9
4.9	3.6	12.0	14.4
5.6	4.5	17.0	28.9
6.4	5.0	20.0	40.0
7.0	5.5	26.5	70.2
7.5	6.0	31.0	96.1
8.3	6.7	36.0	129.6
8.7	7.0	39.0	152.1
9.1	7.3	43.0	184.9
9.8	7.9	45.0	202.5
9.9	7.8	45.0	202.5

D. RETScreen Results

The feasibility study results through RETScreen are given in Table VII.

TABLE. VII Comparison of Performance Metrics for Burrard to King George and Burrard to Waterfront Directions.

Direction	Burrard to Waterfront	Burrard to King George
Capacity Factor (%)	10.84%	25.01%
Internal Rate of Return (%)	-12.1%	-5.7%
Simple Payback Year (yr)	133	50.2
Carbon Emission Reduction (%)	93%	93%

IV. Discussion

A. Phase Analysis and Validation of Train-Induced Flows

Train-induced airflow within station tunnels can be effectively characterized by four consecutive phases:

- **Pre-Compression(1)**: The approaching train causes a slight pressure build-up, resulting in a modest wind speed increase.
- **Piston Effect(2)**: A sudden velocity spike occurs as the train enters the tunnel.
- **Slipstream(3)**: Sustained moderately high wind speeds accompany the train's body as it moves past.
- **Wake(4&5)**: Turbulence and eddies persist after the train's departure, with wind speeds gradually diminishing over time.

These phases, illustrated in Figure 5, are temporally consistent across routes despite variations in station geometry. Peak wind speeds differ, reaching approximately 6 m/s on the Burrard-to-King George route compared to 3 m/s on the Burrard-to-Waterfront route (Figure 3), indicating that station design affects the intensity of the piston effect without altering its overall duration.

To validate this segmentation, FFT analyses were conducted on airflow data across routes with different train dispatch intervals. The Burrard-to-Waterfront route, operating at a 2.5–3 minute dispatch interval, exhibited a dominant frequency of approximately 0.02855 Hz. Similarly, the Burrard-to-King George route, with a 4-minute dispatch interval, showed a dominant frequency of 0.0250 Hz.

In both cases, the periodicity closely aligns with one-fourth of the overall train dispatch frequency, validating the four-phase framework. This consistency across different routes and geometries highlights the robust and repeatable nature of the airflow phases, establishing the segmentation approach as a reliable methodology for analyzing and harnessing train-induced wind energy.

B. Power Density

Based on the calculations and simulation results, the average wind power density for each direction is 2.44 W/m^2 and 7.11 W/m^2, respectively. Considering Betz's limit, the maximum available energy is estimated to range from 1.46 W/m^2 to 4.27 W/m^2. Using a specific wind turbine tested under similar conditions, the expected output is between 343 mW and 1000 mW. However, experimental results achieved only 202.5 mW, consistent with findings from other studies [18].

This indicates that the motor efficiency ranges from 20.3% to 59.0%, which is significantly lower than industrial standards [19].

C. Feasibility Study

The economic analysis reveals stark contrasts between the two routes. The Burrard to King George direction demonstrates greater promise, with a capacity factor of 25.01%—over double that of the Burrard to Waterfront route (10.84%). This disparity arises from differences in tunnel geometry and train dispatch intervals, which amplify airflow velocities on the King George route. Despite this advantage, both projects face prohibitive financial barriers: the IRR remains negative (-5.7% and -12.1%, respectively), and payback periods span 50.2 and 133 years—far exceeding the typical 20-year lifespan of wind energy systems. These metrics underscore a critical mismatch between installation costs ($10,000/kW) and energy output, driven by the sporadic, low-velocity airflow inherent to subway environments.

Notably, the capacity factors fall significantly short of conventional wind farms (30–40%), where steady, high-speed winds justify upfront investments. In metro tunnels, frequent interruptions between train passages limit energy generation to brief, intense pulses, reducing overall system efficiency. While the proposed 500-turbine array achieves a commendable 93% carbon emission reduction—aligning with Vancouver's climate goals—the economic impracticality highlights a need for cost-reduction strategies.

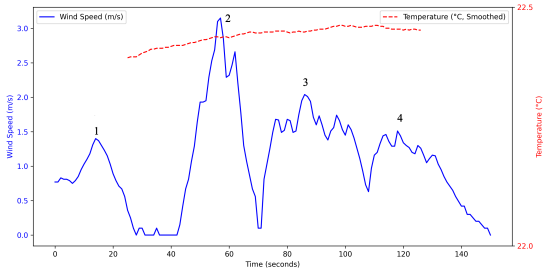

(a)Burrard to Waterfront

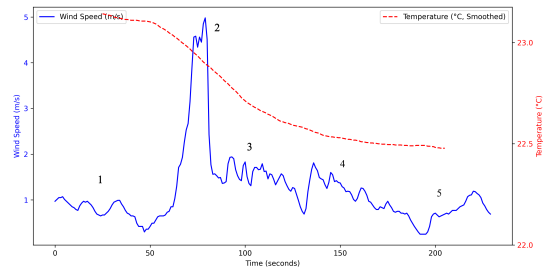

(b)Burrard to King George

Figure. 5: One Dispatch Phase on Different routes

V. Conclusion

This study demonstrates that train-induced airflow in Vancouver's SkyTrain tunnels can be harnessed for renewable energy generation, offering measurable environmental benefits. Field data and statistical modeling revealed distinct airflow phases—pre-compression, piston effect, slipstream, and wake—with peak velocities up to 6 m/s, validating the technical feasibility of energy capture. However, experimental testing of an Archimedes-type turbine yielded limited outputs (202.5 mW), highlighting efficiency challenges. Economic analysis via RETScreen further underscored barriers, with capacity factors below 25% and payback periods exceeding 50

years, rendering the project financially unviable under current conditions.

Despite economic hurdles, the environmental potential is significant, with carbon emission reductions of 93%. To advance implementation, future work must prioritize innovations in turbine aerodynamics, energy storage integration, and policy incentives to improve cost-effectiveness. This research provides a methodological blueprint for urban transit networks globally, emphasizing the dual role of infrastructure in mobility and sustainability. With targeted advancements, train-induced wind energy could complement municipal clean-energy portfolios, reducing the carbon footprint of public transportation while leveraging existing urban systems.

Author Contributions

Both authors Lisha Tan and Yunbo Nie contributed equally to the research and preparation of this paper. Dr. Mohammad Rahnama provided supervision and critical review throughout the research process.

References

[1] D. Cross, B. Hughes, D. Ingham, and L. Ma, "Enhancing the piston effect in underground railway tunnels," *Tunnelling and Underground Space Technology*, vol. 61, pp. 71–81, Jan. 2017.

[2] T. Rachmanta, A. Basid, and H. Asri, "The utilization of moving train as an alternative energy source in railways with Savonius wind turbine," *Journal of Physics: Conference Series*, vol. 1700, p. 012051, 2020.

[3] S. Liu, Y. Li, H. Wang, and L. Wang, "Modified Savonius wind turbine for the application of energy harvesting from train-induced wind in subway tunnel," *Renewable Energy*, vol. 136, pp. 1044–1056, 2019.

[4] S. Liu, B. Zhao, Y. Li, H. Wang, and L. Wang, "A novel wind energy harvesting system for the application of airflow-induced vibration from the train-induced wind in subway tunnels," *Energy*, vol. 230, p. 120446, 2021.

[5] Hi-VAWT Technology Corp., "DS-300 Vertical Axis Wind Turbine," [Online]. Available: http://www.hi-vawt.com.tw/en/ds300w.html [Accessed: Nov. 1, 2024].

[6] Inverter.com, "ATO-X3-200 Helical Vertical Axis Wind Turbine," [Online]. Available: https://www.inverter.com/200w-vertical-axis-wind-turbine [Accessed: Nov. 1, 2024].

[7] ATO, "ATO-X3-100 Vertical Axis Wind Turbine," [Online]. Available: https://www.ato.com/100w-vertical-axis-wind-turbine [Accessed: Nov. 1, 2024].

[8] Shenzhen ErTuan Turbine Generator Technology Factory, "12V/24V Small Shaft Wind Turbine XTL-R1-100W Energy System 12V/24V Generator Set Vertical Alternate Wind Turbine," [Online]. Available: https://www.turbinesgenerator.com/sale-16603034-12v-24v-small-shaft-wind-turbine-xtl-r1-100w-energy-system-12v-24v-generator-set-vertical-alternate-.html [Accessed: Nov. 1, 2024].

[9] PUMARS, "HS-100 Horizontal Wind Turbine," [Online]. Available: Vertical-axis-wind-turbine-technical-specifications.pdf [Accessed: Nov. 1, 2024].

[10] Future Sustainability, "50w 12v 24v Vertical Axis Helix Mini Permanent Magnet Windmill Generator Free Energy Off on Grid for Home Hybrid System FS-50," [Online]. Available: https://m.flytpower.com/50w-12v-24v-vertical-axis-helix-mini-permanent-magnet-windmill-generator-free-energy-off-on-grid-for-home-hybrid-system-fs-50-product [Accessed: Nov. 1, 2024].

[11] 54Energy, "Mini Vertical Axis Wind Turbine Generator 10W 12VDC Windmill Generator Max 15w 5 Blades High Quality for Household Street," [Online]. Available: https://54energy.net/products/mini-vertical-axis-wind-turbine-generator-10w-12vdc-windmill-generator-max-15w-5-blades-high-quality-for-household-street [Accessed: Nov. 2, 2024].

[12] Leading Edge Power, "LE-v50 Extreme Vertical Axis Wind Turbine (12/24/48V)," [Online]. Available: https://www.leadingedgepower.com/le-v50-extreme-vertical-axis-wind-turbine-12-24-48v-1486339.html [Accessed: Nov. 2, 2024].

[13] Inverter.com, "ATO-WT-S100 Horizontal Axis Wind Turbine," [Online]. Available: https://www.inverter.com/100w-wind-turbine [Accessed: Nov. 1, 2024].

[14] Amazon, "10W Micro Spiral Wind Generator Model Permanent Magnet Generator DIY White Wind Turbine Model Breeze Start Generator Light with LED Light," [Online]. Available: https://www.amazon.ca/gp/product/B0CCVSGSZS [Accessed: Nov. 1, 2024].

[15] U SC Respect, "AWM-750D-150W Archimedes Spiral Wind Turbine," [Online]. Available: https://thearchimedes.com/products [Accessed: Nov. 1, 2024].

[16] Changzhou Shengshijia Electronic Co., Ltd., "50W Horizontal 3 Blades Mini Windmill (SHJ-50S)," [Online]. Available: https://cctvcamerachina.en.made-in-china.com/product/lXtEmUYDFLWG/China-50W-Horizontal-3-Blades-Mini-Windmill-SHJ-50S-.html [Accessed: Nov. 2, 2024].

[17] L. Martino, D. Luengo, and J. Míguez, "Accept–Reject methods," *Statistics and Computing/Statistics and Computing*, 2018, pp. 65–113.

[18] M. Rahman, M. Salauddin, P. Maharjan, M.S. Rasel, H. Cho, and J. Park "Natural wind-driven ultra-compact and highly efficient hybridized nanogenerator for self-sustained wireless environmental monitoring system" Nano Energy, Vol. 57, pp. 256–268, 2019

[19] National Electrical Manufacturers Association "ANSUNEMA MG 1-2021 Motors and Generators" American National Standard, 2022